Comparison of ^{18}F-Fluoroethyltyrosine PET and Sodium MRI in Cerebral Gliomas: a pilot study

Aliaksandra Shymanskaya[a,†], Wieland A. Worthoff[a,†], Gabriele Stoffels[a], Johannes Lindemeyer[a], Bernd Neumaier[a], Philipp Lohmann[a], Norbert Galldiks[a,b,c], Karl-Josef Langen[a,d,e], and N. Jon Shah[a,e,f]

[a]Institute of Neuroscience and Medicine (3, 4, 5, 11) Forschungszentrum Jülich, Jülich, Germany
[b]Department of Neurology, University of Cologne, Cologne, Germany, Germany
[c]Center of Integrated Oncology (CIO), Universities of Bonn and Cologne, Cologne, Germany
[d]Department of Nuclear Medicine, RWTH Aachen University, Aachen, Germany
[e]Jülich-Aachen Research Alliance (JARA) – Section JARA-Brain, Aachen, Germany
[f]Department of Neurology, RWTH Aachen University, Aachen, Germany

*Address correspondence to:
Dr. Wieland A. Worthoff,
Institute of Neuroscience and Medicine - 4
Forschungszentrum Jülich GmbH
52425 Jülich
Germany
Tel.: +49 (0) 2461 61 8772
Fax: +49 (0) 2461 61 1919
Email: w.worthoff@fz-juelich.de

† both authors contributed equally

Manuscript Category: Article

Abstract

Purpose Positron emission tomography **(**PET) using O-(2-[^{18}F]fluoroethyl)-L-tyrosine ([^{18}F]FET) improves the diagnostics of cerebral gliomas compared to conventional magnetic resonance imaging (MRI). Sodium MRI is an evolving method to assess tumor metabolism. In this pilot study we explored the relationship of [^{18}F]FET-PET and sodium MRI in patients with cerebral gliomas in relation to the mutational status of the enzyme isocitrate dehydrogenase (IDH).

Procedures Ten patients with untreated cerebral gliomas and one patient with a recurrent glioblastoma (GBM) were investigated by dynamic [^{18}F]FET-PET and sodium MRI using an enhanced simultaneous single-quantum and triple-quantum-filtered imaging of ^{23}Na (SISTINA) sequence to estimate total (NaT), weighted non-restricted (NaNR, mainly extracellular) and restricted (NaR, mainly intracellular) sodium in tumors and normal brain tissue. [^{18}F]FET uptake and sodium parameters in tumors with a different IDH mutational status were compared. After biopsy or resection, histology and the IDH mutational status were determined neuropathologically.

Results NaT ($p=0.05$), tumor-to-brain ratios (TBR) of NaT ($p=0.02$), NaNR ($p=0.003$), and the ratio of NaT/NaR ($p<0.001$) were significantly higher in IDH mutated than in IDH wildtype gliomas ($n=5$ patients each) while NaR was significantly lower in IDH mutated gliomas ($p=0.01$). [^{18}F]FET parameters (TBR, time-to-peak) were not predictive for IDH status in this small cohort of patients. There was no obvious relationship between sodium distribution and [^{18}F]FET uptake. The patient with a recurrent GBM exhibited an additional radiation injury with strong abnormalities in sodium MRI.

Conclusions Sodium MRI appears to be more strongly related to the IDH mutational status than are [^{18}F]FET-PET parameters. A further evaluation of the combination of the two methods in a larger group of high- and low-grade gliomas seems promising.

Keywords: MRI, FET-PET, sodium imaging, gliomas, IDH mutational status

Introduction

Cerebral gliomas are the most common primary brain tumors with an incidence of 5 - 6 per 100,000 persons per year [1]. Despite intensive efforts to improve therapy, the majority of gliomas are associated with a poor prognosis [2]. The molecular genetic profile of cerebral gliomas such as the gene mutation encoding for the isocitrate dehydrogenase enzyme (IDH) is of increasing importance for treatment strategy [3]. Since this requires invasive tissue sampling, there is also a great interest in obtaining such information using modern molecular imaging techniques [4]. Initial studies have shown that a combination of conventional magnetic resonance imaging (MRI) and advanced MRI methods such as perfusion weighted imaging (PWI) and diffusion weighted imaging (DWI) may predict IDH mutation status non-invasively [5-6]. Furthermore, recent studies report that amino acid positron emission tomography (PET) is also highly predictive of IDH mutational status and that dynamic PET using O-(2-[^{18}F]fluoroethyl)-L-tyrosine ([^{18}F]FET), especially, are independent predictors of survival and superior to molecular parameters in terms of patient prognosis in some subgroups [7-12].

Another evolving MR method that may substantially contribute to the characterization of brain tumors is sodium (^{23}Na) MRI. Sodium is a most important electrolyte which plays an essential role in human cell physiology [13] and its distribution reflects the functional status of the sodium-potassium pump and sodium channels in cells [14]. The concentration gradient between the intra- and the extracellular space is maintained mainly by the energy dependent sodium-potassium pump (Na^+/K^+-Adenosine triphosphate (ATPase)) [15]. Any harm to the cell membrane integrity or disturbances of energy metabolism can lead to impairment of the sodium-potassium pump with the consequence of increasing intracellular sodium concentration, change in cell volume, and malfunction of cells [16-18]. The chemical environment of sodium ions inside and outside cells determines relaxation behavior of sodium ions thus generating MR contrasts. A number of techniques are under development to differentiate MR signals originating from intra- and extracellular sodium ions. Earlier studies did not allow this distinction, which made it difficult to detect alterations of intracellular sodium due to a high contribution from the extracellular compartment. In this study, a technique using enhanced simultaneous single-quantum and triple-quantum-filtered imaging of ^{23}Na (enhanced SISTINA) developed at our institute has been applied, allowing simultaneous acquisition of signal originating from restricted and non-restricted sodium [19-20]. While the so-called single quantum coherences (SQCs) develop in both areas with restricted (mostly intracellular sodium) and non-restricted sodium (mostly extracellular sodium), triple quantum

coherences (TQCs) evolve in a restricted environment only [21], and can be measured when an appropriate pulse sequence is applied [22-23]. SISTINA sequences allow simultaneous acquisition of signal originating from restricted and non-restricted sodium [19-20].

Initial studies on human brain tumors indicated that the measurement of total sodium content could provide information on tumor response during radiotherapy and chemotherapy [16, 24]. Furthermore, a recent study using an ultra-high field MRI (7T) in brain tumor patients has reported that the ratio of intracellular and extracellular sodium in cerebral gliomas has a high predictive value for the gene mutation encoding for the isocitrate dehydrogenase enzyme (IDH) [25]. An IDH mutation is an important molecular marker in the World Health Organization (WHO) classification of brain tumors of 2016 [3]. Patients with an IDH mutation have an improved outcome than do patients with IDH wildtype (wt) gliomas. Similarly, a relationship between [^{18}F]FET-PET parameters and IDH mutation has been reported [8-10]. The aim of this pilot study was to explore the relationship of metabolic parameters derived from [^{18}F]FET-PET and disturbances of restricted and unrestricted sodium in patients with cerebral gliomas with a different IDH mutational status.

Materials and Methods:

Patients

11 patients, referred to the Department of Nuclear Medicine of the University Clinic of Aachen, were investigated by [^{18}F]FET-PET for brain tumor assessment and had additional morphological imaging in a 4T MRI scanner for comparison with [^{18}F]FET-PET. Sodium imaging was offered in addition to conventional MR sequences. All subjects gave written informed consent prior to [^{18}F]FET-PET and MR imaging. All 11 patients had a neuropathological diagnosis based on the 2016 WHO classification [3] (4 female, age 43±12, and 7 male, age 53±15). Five patients had an untreated IDH mutated glioma (1 astrocytoma WHO Grade II; 3 anaplastic astrocytoma WHO grade III; 1 glioblastoma WHO grade IV), five patients an untreated IDH wildtype glioma (3 anaplastic glioma WHO Grade III; 1 diffuse midline glioma WHO IV; 1 glioblastoma WHO grade IV), and one patient a pretreated multifocal glioblastoma WHO grade IV (IDH wildtype). The latter patient showed a recurrent tumor and a radiation injury in different brain areas as confirmed by further follow-up. Given its retrospective nature, the local ethics committee of the University of Aachen waived the requirement for additional approval. The study adheres to the standards established in the declaration of Helsinki. Further details about the patient cohort are provided in Table 1.

[^{18}F]FET-PET

The amino acid [^{18}F]FET was produced as described previously [26-27]. According to the German guidelines for brain tumor imaging using radiolabeled amino acid analogues, all patients had been fasting for at least 12h before PET scanning [28]. Dynamic PET studies were acquired up to 50min after intravenous injection of approximately 200MBq [^{18}F]FET on an ECAT EXACT HR+ scanner (Siemens Medical Systems, Inc.) in 3-dimensional mode (32 rings; axial field of view, 15.5cm). The reconstructed dynamic dataset consisted of 16 time frames (5x1min; 5x3min; 6x5min). Attenuation correction was based on a 10min transmission scan measured with three rotating line sources (^{68}Ge/^{68}Ga). Data were corrected for random and scattered coincidences, and dead time prior to iterative reconstruction of 63

image planes using the OSEM algorithm (16 subsets, 6 iterations). The reconstructed image resolution was approximately 5.5mm [29].

[^{18}F]FET-PET scans were coregistered with conventional MRI (see below) and evaluated by region-of-interest (ROI) using MPI tool (Version 3.28, ATV, Kerpen, Germany). For tumors with increased [^{18}F]FET uptake, the transaxial slice showing the highest lesion intensity was chosen and a circular ROI with a diameter of 1.6cm was drawn automatically around the lesion maximum, making tumour evaluation independent on the size of the lesion. A larger reference ROI was placed in the contralateral hemisphere in the normal-appearing brain including white and grey matter [30]. Since some of the lesions exhibited an [^{18}F]FET uptake similar to that of the normal brain tissue, an ROI analysis based on threshold values was not possible. Therefore, a representative irregular ROI was placed manually on the area of signal abnormality in the T_1- and T_2-weighted transversal MR scan and transferred to the coregistered [^{18}F]FET-PET scan in each case. [^{18}F]FET uptake was expressed as standardized uptake value (SUV) by dividing the radioactivity (Bq/mL) in the tissue by the radioactivity injected per gram of body weight. Mean and maximal tumor-to-brain ratios (TBR_{mean},TBR_{max}) were calculated on summed [^{18}F]FET-PET images from 20-40min post injection by dividing the mean and maximal ROI value (Bq/ml) of the lesion by the mean ROI value of normal brain. If the TBR_{max} was higher than the threshold of 1.6, the lesion was considered [^{18}F]FET positive [31]. Time activity curves (TAC) were generated by application of the ROIs to the entire dynamic data set. Time-to-peak (TTP; time in minutes from the beginning of the dynamic acquisition up to the maximum SUV of the lesion) was determined. TTP earlier than 17.5min after injection was rated as early TTP and later than 17.5min after injection as late TTP [8].

Sodium MR-Imaging

Sodium images were acquired on a home-built 4T MRI scanner based around a Siemens console with a dual-tuned Na/H birdcage coil (Rapid Biomed, Germany) using an enhanced SISTINA sequence [20]. Enhanced SISTINA consists of a triple quantum filter (TQF) with an ultrashort echo time (UTE) readout train after the first 90° pulse, which gives total sodium concentration weighting, and a Cartesian, multiple gradient echo (MGRE) readout after the third 90° pulse, which yields information about single-quantum (SQ) and triple-quantum (TQ) coherences after application of appropriate phase cycle [32].

The parameters used for simultaneous acquisition of UTE, SQ and TQ images are provided in supplementary material Table A1, sequence timing and echo spacing were the same as in [20]. The repetition time was 150ms, yielding a measurement time of approximately 10min. Multiple GREs were acquired for relaxometry measurements. The data were regridded to 2.5mm isotropic resolution. Further details on k-space acquisition and data postprocessing, calculation of unbiased signal-to-noise ratio (SNR) in the sodium images and correction procedures have been reported previously [33].

The conventional MR images acquired at 4T were coregistered with [^{18}F]FET-PET scans and subsequently with sodium images, as well as between UTE and Cartesian sodium images using the FSL library (FMRIB, Oxford, UK) [34-36]. Three regions were segmented manually using the normal proton images: the tumor area, which corresponds either to increased [^{18}F]FET uptake in PET uptake or to T_1- or T_2-signal abnormalities in case of indifferent [^{18}F]FET uptake, a reference area in the normal-appearing contralateral brain tissue, and normally appearing white matter.

Sodium concentration, NaT, in the ROIs was determined using $NaT_{ROI} = SNR_{ROI} \cdot SNR_{ref}^{-1} \cdot NaT_{ref}$, with the SNR in the sodium UTE images (SNR_{ROI}), a sodium signal from the vitreous humor of the eyes (SNR_{ref}, taken as a reference), and NaT_{ref}=135mmol/L, which is an approximation from the literature [37-39].

Total sodium concentration, NaT, signal from sodium ions with predominantly non-restricted mobility (NaNR = SNR of SQ weighted images), signal from sodium ions with predominantly restricted mobility (NaR = SNR of TQ-weighted images) were estimated. Furthermore, the TBRs of the signals relative to healthy contralateral tissue and the ratio between NaT and NaR were determined. Complete data for the patients is given in Table 2 and in supplementary materials.

Statistical Analysis

Descriptive statistics for sodium and [^{18}F]FET parameters are provided as mean and standard deviation for all patients as well as for IDH mutated and IDH wildtype groups separately. To compare sodium MRI and [^{18}F]FET-PET parameters in patients with and without IDH mutation, the Student *t*-test for independent samples was used. The Wilcoxon test was used when variables were not normally distributed. Pearson Product Correlations were performed for testing correlations between two variables due to data normality (Shapiro-Wilk test delivered $p>0.05$). P values of 0.05 or less were considered significant. Statistical analyses were performed using SigmaPlot software (SigmaPlot Version 11.0, Systat Software Inc., San Jose, CA) and PASW Statistics software (Release 22.0.0, SPSS Inc., Chicago, IL, USA). No correction for multiple testing was applied.

Results

Sodium Imaging

Visual evaluation of the sodium images of the patients revealed a prominent relative increase of NaT and NaNR compared to the normal brain and a decrease of NaR in 4 of 5 patients with IDH mutation. A typical example is shown in Figure 1a (patient 2). In contrast, this pattern was not observed in any of the 5 IDH wildtype patients (Table 1). A representative example is shown in Figure 2a (patient 7). Quantitative evaluation showed that the group of tumors with IDH mutation showed a significantly higher NaT than IDH wildtype gliomas (58.7±10.4mmol/L versus 40.5±24.0mmol/L; $p=0.05$), a significantly higher TBR of NaT (2.16±0.12 versus 1.48±0.53; $p=0.02$) and a significantly higher TBR of NaNR (2.72±0.68 versus 1.27±0.32, $p=0.003$). Furthermore, TBR of NaR was significantly decreased in IDH mutated gliomas compared with IDH wildtype (0.54±0.08 versus 0.82±0.18, $p=0.01$). Correspondingly, the ratio NaT/NaR was significantly different between the two groups (4.09±0.64 versus 1.85±0.66, $p=0.001$). The radiation injury of the pretreated patient showed considerable stronger abnormality in sodium imaging (NaT increased by 28% and NaNR increased by 42%, NaR decreased by 15%) than the recurrent glioblastoma (Figure 4).

[18]FFET PET and comparison with sodium MRI

In contrast to the results with sodium imaging, quantitative evaluation of [^{18}F]FET uptake parameters showed no significant difference between IDH mutated and IDH wildtype gliomas, which is not in line with the results in the literature obtained in larger groups of patients (Table 2). In the group of IDH mutated gliomas, two patients showed an increased [^{18}F]FET uptake and all tumors in this group showed a late TTP. In the group of IDH wildtype tumors, two patients showed low [^{18}F]FET uptake and three patients showed a late TTP, which is usually associated with an IDH mutation (Table 1). Furthermore, there was no obvious relationship between [^{18}F]FET uptake and sodium imaging. Cases with low [^{18}F]FET uptake showed both abnormal and inconspicuous sodium distribution (Figure 1a and Figure 2a). In contrast, high [^{18}F]FET uptake was found in both tumors with abnormal and inconspicuous sodium distribution (Figure 1b and Figure 2b). In the latter patient with an IDH wildtype, however, the [^{18}F]FET TAC showed an early TTP peak followed by a constant descent, which is indicative for a highly malignant tumor. Correlation analysis between sodium MRI and [^{18}F]FET-PET parameters in the tumors yielded no significant correlation except a weak negative relationship between the TBR_{max} of [^{18}F]FET uptake and NaT (Figure 3).

Discussion

Sodium MRI is an evolving method in this field and thus far, only little data are available with this method in relation to molecular markers of gliomas. A recent study by Biller et al. [25] reported that the ratio of ^{23}Na ions with restricted mobility and total sodium concentration (NaR/NaT) was significantly lower in gliomas with IDH mutation than in IDH wildtype gliomas. In that study, the NaR/NaT ratio was an independent predictor of progression free survival [25]. We here used the enhanced SISTINA method, which provides further insights into the intratumoral distribution of ^{23}Na ions with restricted and unrestricted mobility in relation to the IDH mutation status of gliomas. We observed that 80% of IDH mutated gliomas exhibited a significant increase of total ^{23}Na concentration NaT, a relative increase of ^{23}Na ions with unrestricted mobility (mainly extracellular, NaNR) and a relative decrease of ^{23}Na ions with restricted mobility (mainly intracellular, NaR). In contrast, none of the IDH wildtype gliomas showed this pattern and all parameters of sodium imaging were significantly different compared with

IDH mutated gliomas although the sample size was relatively small. These findings are in line with the observations by Biller et al. mentioned above [25]. Similar results have also been reported in a recent study which, however, included one single case of a IDH wildtype glioma only [40]. Thus, the results of this pilot study support the hypothesis that abnormalities in sodium imaging are related to the molecular profile of gliomas such as the IDH mutation status, which is related to the aggressiveness of the tumor. In contrast to sodium imaging, in this small series of patients [^{18}F]FET-PET parameters did not show differences between IDH mutated and IDH wildtype gliomas, which is contrary to the results observed in larger series of patients [8-10]. The lack of statistical significance may be explained by the relatively small group of patients, but the apparent discrepancy with sodium imaging gives the impression that advanced sodium imaging is a very sensitive method with regard to this issue and is possibly superior to [^{18}F]FET-PET. Furthermore, our data give rise to the assumption that the sodium signal and amino acid transport abnormalities are not closely linked to each other but reflect different metabolic properties of gliomas.

The importance of sodium metabolism in the development of gliomas has gained increasing interest in recent years. It has been shown that glioblastoma patients with mutations in sodium channels show a significantly shorter survival compared to patients with no sodium channel mutations [41-42]. Upregulation of the Na^+/H^+ exchanger isoform 1 (NHE1), which leads to increased intracellular sodium and increased cellular pH, has been implicated in promoting glioma proliferation, invasion and resistance to temozolomide therapy [43-44]. An increase in intracellular sodium concentration which is more pronounced in rapidly dividing cells [45] may indicate a breakdown of the Na^+/K^+-ATPase and/or Na^+ cotransporters. Nevertheless, the IDH mutated gliomas showed a higher total sodium concentration than in the normal brain (Figures 1a and 1b), which is probably caused by an increased extracellular volume. These relationships in gliomas with different IDH genotype are elucidated for the first time by the SISTINA method used here, which allows the simultaneous detection of the restricted and non-restricted sodium. It is tempting to speculate that IDH mutated gliomas exhibit either a lower amount of restricted, mainly intracellular sodium, or a lower level cellularity than IDH wildtype gliomas, suggesting that the extra/intracellular sodium concentration gradient is better maintained in these tumors (Figures 1 and 2). Confirmation of this hypothesis, however, requires a significantly larger population and, in particular, the inclusion of a larger fraction of patients with WHO grade II gliomas.

In our study, there was also a case of a recurrent glioblastoma patient with radiation injury, as confirmed

by repeated PET/MR imaging after 5 months (patient 11). Interestingly, the radiation injury showed considerable stronger abnormality in sodium imaging (increased NaT and NaNR, decreased NaR) than the recurrent glioblastoma (Figure 4). Our study has several limitations. The number of patients in this pilot study is rather small and the distribution of WHO grades of the tumors in the different groups with and without IDH mutation is not completely identical. Therefore, a confirmation of the results in a larger collective with homogeneous and more representative collectives is needed. Some caution is advised when comparing the results of sodium imaging with the literature, because the methods of MR imaging are different [13]. A relative decrease in the concentration of sodium ions with restricted mobility may also be caused by an increase of the intracellular space, or the increase of extracellular space, e.g., by edema. Furthermore, sodium MRI suffers from low SNR and low resolution, which will be improved in the near future by the increasing availability of ultra-high field scanners at 7T [32, 46] and higher [47-48]. The possible PVE from the high SNR regions such as ventricles and choroid plexus are however balanced by the appropriate choice of the reference ROIs. Nevertheless, the better image resolution offered by ultra-high field systems, in particular for the acquisition of images with restricted sodium weighting, will significantly enhance the quality of sodium quantification.

Conclusions

In summary, the results of this pilot study support the hypothesis that sodium imaging adds information to predict the IDH mutational status. Sodium MRI appears to be more strongly related to IDH mutational status than are [^{18}F]FET-PET parameters. However, with respect to the excellent performance of [^{18}F]FET-PET in previous reports, a further evaluation of the combination of the two methods in gliomas is promising. Sodium imaging suffers from low SNR and resolution but, as already noted, increasing availability of 7T MRI scanners will allow these methods to be combined and opens new horizons for the non-invasive assessment of the molecular profile of gliomas.

Acknowledgements

The authors thank Petra Engels, Elke Bechholz, Anita Köth, Suzanne Schaden, Elisabeth Theelen, Silke Frensch, Kornelia Frey, Stefan Schwan and Lutz Tellmann for assistance in the patient studies; Johannes Ermert, Silke Grafmüller, Erika Wabbals and Sascha Rehbein for radiosynthesis of [^{18}F]FET.

Compliance of Interest Statement

Funding: None.

Conflict of Interest: The authors declare that they have no conflict of interest.

Ethical approval: All procedures performed in studies involving human participants were in accordance with the ethical standards of the institutional and/or national research committee and with the 1964 Helsinki declaration and its later amendments or comparable ethical standards.

Informed consent: Informed written consent was obtained from all individual participants included in the study.

References

1. Ostrom QT, Gittleman H, Liao P, et al. (2014) CBTRUS statistical report: primary brain and central nervous system tumors diagnosed in the United States in 2007-2011. Neuro Oncol 16 Suppl 4:iv1-63.

2. Ohgaki H, Kleihues P (2005) Population-based studies on incidence, survival rates, and genetic alterations in astrocytic and oligodendroglial gliomas. J Neuropathol Exp Neurol 64:479-489.

3. Louis DN, Perry A, Reifenberger G, et al. (2016) The 2016 World Health Organization Classification of Tumors of the Central Nervous System: a summary. Acta Neuropathol 131:803-820.

4. Langen KJ, Galldiks N, Hattingen E, Shah NJ (2017) Advances in neuro-oncology imaging. Nat Rev Neurol 13:279-289.

5. Leu K, Ott GA, Lai A, et al. (2017) Perfusion and diffusion MRI signatures in histologic and genetic subtypes of WHO grade II-III diffuse gliomas. J Neurooncol 134:177-188.

6. Xing Z, Yang X, She D, Lin Y, Zhang Y, Cao D (2017) Noninvasive Assessment of IDH Mutational Status in World Health Organization Grade II and III Astrocytomas Using DWI and DSC-PWI Combined with Conventional MR Imaging. AJNR Am J Neuroradiol 38:1138-1144.

7. Kunz M, Albert NL, Unterrainer M, et al. (2018) Dynamic 18F-FET PET is a powerful imaging biomarker in gadolinium-negative gliomas. Neuro Oncol.

8. Suchorska B, Giese A, Biczok A, et al. (2018) Identification of time-to-peak on dynamic 18F-FET-PET as a prognostic marker specifically in IDH1/2 mutant diffuse astrocytoma. Neuro Oncol 20:279-288.

9. Verger A, Stoffels G, Bauer EK, et al. (2018) Static and dynamic (18)F-FET PET for the characterization of gliomas defined by IDH and 1p/19q status. Eur J Nucl Med Mol Imaging 45:443-451.

10. Unterrainer M, Winkelmann I, Suchorska B, et al. (2018) Biological tumour volumes of gliomas in early and standard 20-40 min (18)F-FET PET images differ according to IDH mutation status. Eur J Nucl Med Mol Imaging 45:1242-1249.

11. Rohrich M, Huang K, Schrimpf D, et al. (2018) Integrated analysis of dynamic FET PET/CT parameters, histology, and methylation profiling of 44 gliomas. Eur J Nucl Med Mol Imaging 45:1573-1584.

12. Lopci E, Riva M, Olivari L, et al. (2017) Prognostic value of molecular and imaging biomarkers in patients with supratentorial glioma. Eur J Nucl Med Mol Imaging 44:1155-1164.

13. Madelin G, Regatte RR (2013) Biomedical applications of sodium MRI in vivo. J Magn Reson Imaging 38:511-529.

14. Shah NJ, Worthoff WA, Langen KJ (2016) Imaging of sodium in the brain: a brief review. NMR Biomed 29:162-174.

15. Murphy E, Eisner DA (2009) Regulation of intracellular and mitochondrial sodium in health and disease. Circ Res 104:292-303.

16. Thulborn KR, Lu A, Atkinson IC, Damen F, Villano JL (2009) Quantitative sodium MR imaging and sodium bioscales for the management of brain tumors. Neuroimaging Clin N Am 19:615-624.

17. Ouwerkerk R, Bleich KB, Gillen JS, Pomper MG, Bottomley PA (2003) Tissue sodium concentration in human brain tumors as measured with 23Na MR imaging. Radiology 227:529-537.

18. Nagel AM, Bock M, Hartmann C, et al. (2011) The potential of relaxation-weighted sodium magnetic resonance imaging as demonstrated on brain tumors. Invest Radiol 46:539-547.

19. Fiege DP, Romanzetti S, Mirkes CC, Brenner D, Shah NJ (2013) Simultaneous single-quantum and triple-quantum-filtered MRI of 23Na (SISTINA). Magn Reson Med 69:1691-1696.

20. Worthoff WA, Shymanskaya A, Shah NJ (2019) Relaxometry and quantification in simultaneously acquired single and triple quantum filtered sodium MRI. Magnetic Resonance in Medicine 81:303-315.

21. Jaccard G, Wimperis S, Bodenhausen G (1986) Multiple-Quantum Nmr-Spectroscopy of S=3/2 Spins in Isotropic-Phase - a New Probe for Multiexponential Relaxation. Journal of Chemical Physics 85:6282-6293.

22. Keltner JR, Wong ST, Roos MS (1994) Three-dimensional triple-quantum-filtered imaging of 0.012 and 0.024 M sodium-23 using short repetition times. J Magn Reson B 104:219-229.

23. Woessner DE (2001) NMR relaxation of spin-(3)/(2) nuclei: Effects of structure, order, and dynamics in aqueous heterogeneous systems. Concept Magnetic Res 13:294-325.

24. Babsky AM, Zhang H, Hekmatyar SK, Hutchins GD, Bansal N (2007) Monitoring chemotherapeutic response in RIF-1 tumors by single-quantum and triple-quantum-filtered (23)Na MRI, (1)H diffusion-weighted MRI and PET imaging. Magn Reson Imaging 25:1015-1023.

25. Biller A, Badde S, Nagel A, et al. (2016) Improved Brain Tumor Classification by Sodium MR Imaging: Prediction of IDH Mutation Status and Tumor Progression. AJNR Am J Neuroradiol 37:66-73.

26. Hamacher K, Coenen HH (2002) Efficient routine production of the 18F-labelled amino acid O-2-18F fluoroethyl-L-tyrosine. Appl Radiat Isot 57:853-856.

27. Wester HJ, Herz M, Weber W, et al. (1999) Synthesis and radiopharmacology of O-(2-[18F]fluoroethyl)-L-tyrosine for tumor imaging. J Nucl Med 40:205-212.

28. Langen KJ, Bartenstein P, Boecker H, et al. (2011) German guidelines for brain tumour imaging by PET and SPECT using labelled amino acids. Nuklearmedizin 50:167-173.

29. Herzog H, Tellmann L, Hocke C, Pietrzyk U, Casey ME, Kuwert T (2004) NEMA NU2-2001 guided performance evaluation of four siemens ECAT PET scanners. Ieee Transactions on Nuclear Science 51:2662-2669.

30. Unterrainer M, Vettermann F, Brendel M, et al. (2017) Towards standardization of 18F-FET PET imaging: do we need a consistent method of background activity assessment? EJNMMI Res 7:48.

31. Pauleit D, Floeth F, Hamacher K, et al. (2005) O-(2-[18F]fluoroethyl)-L-tyrosine PET combined with MRI improves the diagnostic assessment of cerebral gliomas. Brain 128:678-687.

32. Fiege DP, Romanzetti S, Tse DH, et al. (2013) B0 insensitive multiple-quantum resolved sodium imaging using a phase-rotation scheme. J Magn Reson 228:32-36.

33. Worthoff WA SA, Shah NJ (2018) Relaxometry and quantification in simultaneously acquired single and triple quantum filtered sodium MRI. Magn Reson Med Sci in press.

34. Woolrich MW, Jbabdi S, Patenaude B, et al. (2009) Bayesian analysis of neuroimaging data in FSL. Neuroimage 45:S173-186.

35. Smith SM, Jenkinson M, Woolrich MW, et al. (2004) Advances in functional and structural MR image analysis and implementation as FSL. Neuroimage 23 Suppl 1:S208-219.

36. Jenkinson M, Beckmann CF, Behrens TE, Woolrich MW, Smith SM (2012) Fsl. Neuroimage 62:782-790.

37. Kaufman PL, Adler FH, Levin LA, Alm A (2011) Adler's Physiology of the Eye. Elsevier Health Sciences.

38. Coe JI (1969) Postmortem Chemistries on Human Vitreous Humor. Am J Clin Pathol 51:741-750.

39. Ouwerkerk R, Bleich KB, Gillen JS, Pomper MG, Bottomley PA (2003) Tissue sodium concentration in human brain tumors as measured with Na-23 MR imaging. Radiology 227:529-537.

40. Nunes Neto LP, Madelin G, Sood TP, et al. (2018) Quantitative sodium imaging and gliomas: a feasibility study. Neuroradiology 60:795-802.

41. Joshi AD, Parsons DW, Velculescu VE, Riggins GJ (2011) Sodium ion channel mutations in glioblastoma patients correlate with shorter survival. Mol Cancer 10:17.

42. Wang R, Gurguis CI, Gu W, et al. (2015) Ion channel gene expression predicts survival in glioma patients. Sci Rep 5:11593.

43. Cong D, Zhu W, Shi Y, et al. (2014) Upregulation of NHE1 protein expression enables glioblastoma cells to escape TMZ-mediated toxicity via increased H(+) extrusion, cell migration and survival. Carcinogenesis 35:2014-2024.

44. Zhu W, Carney KE, Pigott VM, et al. (2016) Glioma-mediated microglial activation promotes glioma proliferation and migration: roles of Na+/H+ exchanger isoform 1. Carcinogenesis 37:839-851.

45. Cameron IL, Smith NK, Pool TB, Sparks RL (1980) Intracellular concentration of sodium and other elements as related to mitogenesis and oncogenesis in vivo. Cancer Res 40:1493-1500.

46. Romanzetti S, Mirkes CC, Fiege DP, Celik A, Felder J, Shah NJ (2014) Mapping tissue sodium concentration in the human brain: A comparison of MR sequences at 9.4 Tesla. Neuroimage 96:44-53.

47. Shah NJ (2015) Multimodal neuroimaging in humans at 9.4 T: a technological breakthrough towards an advanced metabolic imaging scanner. Brain Struct Funct 220:1867-1884.

48. Shah NJ, Oros-Peusquens AM, Arrubla J, et al. (2013) Advances in multimodal neuroimaging: hybrid MR-PET and MR-PET-EEG at 3 T and 9.4 T. J Magn Reson 229:101-115.

Figure Legends

Table 1

Group	Pat. No.	Diagnosis	Location	Age, Sex	Gd T_1	^{23}Na NaT	^{23}Na NaNR	^{23}Na NaR	[^{18}F]FET-PET	^{18}FFET-PET early TTP
Untreated IDH mut gliomas	1	A-II	L frontal	34, m	neg.	++	++	– –	–	no
	2	A-III	L temporal	35, f	neg.	++	++	– –	–	no
	3	A-III	L fronto-temp.	29, f	neg.	++	++	– –	–	no
	4	A-III	L frontal	54, f	neg.	+	–	–	++	no
	5	GBM-IV	L frontal insular	38, m	pos.	++	++	– –	++	no
Untreated IDH wt gliomas	6	A-III	L insular	51, m	neg.	–	–	–	–	no
	7	DMG-IV	R postero-lateral	52, f	neg.	+	–	–	–	no
	8	A-III	L temporal	66, m	neg.	+	–	+	++	no
	9	A-III	R basal ganglia	78, m	pos.	+	–	–	++	yes
	10	GBM-IV	L temporal	56, m	neg.	–	–	–	++	no
Pretreated IDH-wt GBM	11	Rec-GBM Radiation injury	R parietal	50, m	pos.	+	+	–	+	no
			L precentral		pos.	+	++	– –	–	no

TABLE 1: IDH mut =gliomas with mutation of the isocytrate dehydrogenase gene, IDH wt = wildtype, gliomas without mutation of the isocitrate dehydrogenase gene, A = Astrocytoma, GBM = Glioblastoma, DMG = Diffuse midline glioma H3 K27M-mutant, I-IV = WHO grades, Rec = recurrent, NaT = total sodium concentration, NaNR = non-restricted sodium SNR (mainly extracellular), NaR = restricted sodium SNR (mainly intracellular), early TTP = time to peak of the time activity curve earlier than 17.5 min p.i. (yes/no), "++" strongly increased signal, "+" slightly increased signal, " – " equal to background, "– –" decreased signal.

Table 2

Group	Patient	Sodium MRI					[^{18}F]FET-PET		
	No	NaT [mmol/L]	NaT (TBR)	NaNR (TBR)	NaR (TBR)	NaT/NaR	TBR_{mean}	TBR_{max}	TTP (min)
IDH mut	1	51.4	2.00	2.22	0.66	3.03	1.0	1.4	40
	2	66.5	2.17	3.73	0.46	4.72	1.4	1.6	40
	3	66.2	2.33	1.98	0.55	4.24	0.4	1.1	40
	4	43.9	2.17	2.81	0.53	4.09	2.3	3.2	40
	5	65.4	2.14	2.86	0.49	4.37	2.6	3.4	35
Mean N=5:		58.7±10.4	2.16±0.12	2.72±0.68	0.54±0.08	4.09±0.64	1.54±0.91	2.14±1.08	39±2
IDH wt	6	57.1	1.62	1.46	0.83	1.95	1.0	1.0	40
	7	44.1	2.27	1.43	0.78	2.91	1.3	2.0	25
	8	48.9	1.52	1.55	1.05	1.45	2.0	2.8	40
	9	23.9	0.98	1.16	0.56	1.75	3.3	5.6	7
	10	28.3	1.01	0.77	0.86	1.17	2.2	3.1	25
Mean N=5:		40.5±14.0	1.48±0.53	1.27±0.32	0.82±0.18	1.85±0.66	1.96±0.90	2.90±1.71	27±13
P-value		**0.05**	**0.02**	**0.003**	**0.01**	**<0.001**	**0.48**	**0.78**	**0.10**
Recurrence	11	44.4	2.20	1.91	0.71	3.10	2.0	3.1	25
Radiation injury		57.1	2.82	2.71	0.60	4.70	1.3	1.9	40

TABLE 2: IDH mut =gliomas with mutation of the isocytrate dehydrogenase gene, IDH wt = wild type, gliomas without mutation of the isocitrate dehydrogenase gene, NaT = total sodium concentration, NaNR = non-restricted sodium SNR (mainly extracellular), NaR = restricted sodium SNR (mainly intracellular), TAC = time activity curve,, TBR_{mean} = mean tumor-to-brain ratio of [^{18}F]FET uptake, TBR_{max} = maximum tumor-to-brain ratio of [^{18}F]FET uptake, TTP = time-to-peak in the time-activity curve of [^{18}F]FET uptake in the tumor.

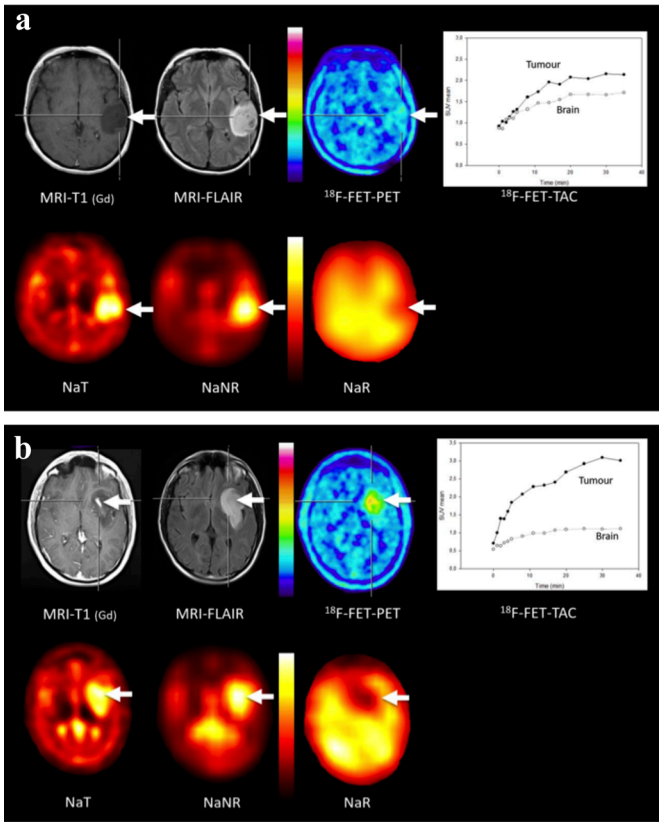

Fig.1: a: MRI and PET of a 35-year-old patient with an IDH mutated anaplastic astrocytoma WHO grade III (white arrow). The tumor shows no contrast enhancement in the T_1-weighted MRI and is clearly delineated in the FLAIR image. [^{18}F]FET-PET shows no significant tracer uptake in the tumor and an increasing time activity curve. Sodium imaging shows increased NaT, increased NaNR, and decreased NaR, which is the typical finding for IDH mutated gliomas. b: MRI and PET of a 38-year-old male patient with an IDH mutated glioblastoma WHO grade IV. The tumor (white arrow) shows focal contrast enhancement in the T_1-weighted MRI and is clearly depicted in the FLAIR image. [^{18}F]FET-PET shows significant tracer uptake in the tumor and an increasing time activity curve. Similar to the IDH mutated glioma in Figure 1a sodium imaging shows increased NaT, increased NaNR, and decreased NaR.

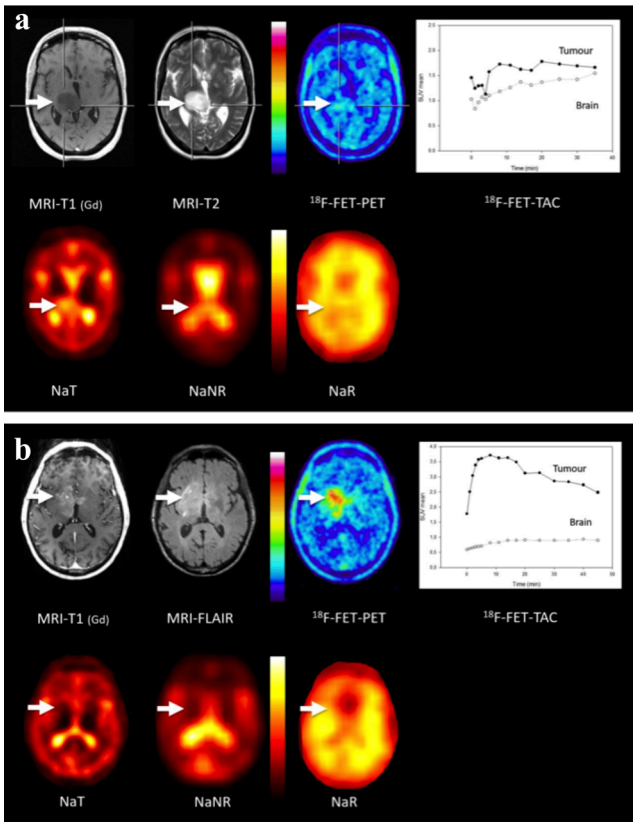

Fig.2: a: MRI and PET of a 52-year-old patient with a diffuse midline glioma WHO grade IV showing IDH wildtype. The tumor (white arrow) shows no contrast enhancement in the T_1-weighted MRI and is clearly depicted in the T_2-weighted MRI. [^{18}F]FET-PET shows no significant tracer uptake in the tumor and an increasing time activity curve. Sodium imaging shows a minor increase of NaT, but no abnormality in NaNR and NaR. b: MRI and PET of a 78-year-old male patient with an IDH wildtype anaplastic astrocytoma WHO grade III in the right basal ganglia. The tumor (white arrows) shows focal contrast enhancement in the T_1-weighted MRI and diffuse abnormalities in the FLAIR image. [^{18}F]FET-PET shows significant tracer uptake in the tumor and a time activity curve with an early peak. Sodium imaging shows no abnormality in NaT, NaNR, or NaR. The signal decrease in the midfrontal area in NaR is due to an artefact caused by air in the ethmoid sinuses.

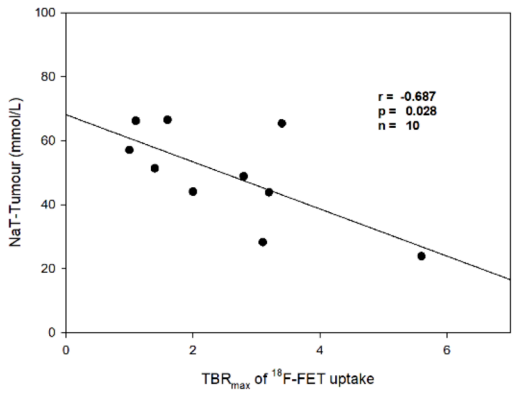

Fig.3: Comparison of the TBR_{max} of [^{18}F]FET uptake in brain tumors and total sodium content. There is a weak inverse relationship, i.e., tumors with increased NaT appear to have lower ^{18}FFET uptake.

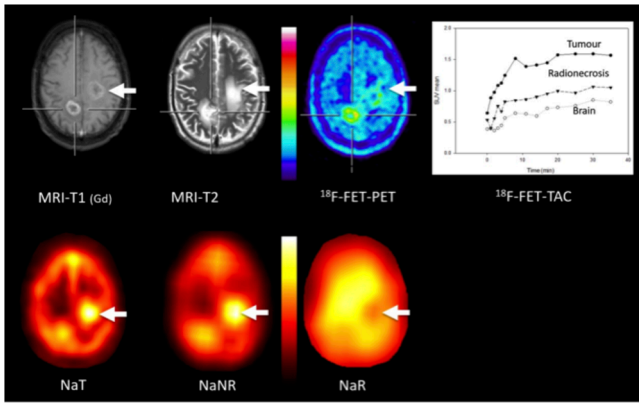

Fig.4: MRI and PET of a 50-year-old male patient with a recurrent IDH wildtype glioblastoma WHO grade IV in the right parietal lobe and a radiation injury on the contralateral side (white arrows), both confirmed by follow-up. Both lesions exhibit contrast enhancement in the T_1-weighted MRI and diffuse abnormalities in the T_2-weigthed MRI. [^{18}F]FET-PET is positive in the recurrent tumor and negative in the necrosis. Sodium imaging shows more prominent abnormalities in the radionecrosis.